Pure Appl. Geophys. 172 (2015), 3455–3472

DOI 10.1007/s00024-015-1049-2

Pure and Applied Geophysics

Parallel Implementation of Dispersive Tsunami Wave Modeling with a Nesting Algorithm for the 2011 Tohoku Tsunami

Toshitaka Baba,[1,3] Narumi Takahashi,[1] Yoshiyuki Kaneda,[1] Kazuto Ando,[1] Daisuke Matsuoka,[1] and Toshihiro Kato[2]

Abstract—Because of improvements in offshore tsunami observation technology, dispersion phenomena during tsunami propagation have often been observed in recent tsunamis, for example the 2004 Indian Ocean and 2011 Tohoku tsunamis. The dispersive propagation of tsunamis can be simulated by use of the Boussinesq model, but the model demands many computational resources. However, rapid progress has been made in parallel computing technology. In this study, we investigated a parallelized approach for dispersive tsunami wave modeling. Our new parallel software solves the nonlinear Boussinesq dispersive equations in spherical coordinates. A variable nested algorithm was used to increase spatial resolution in the target region. The software can also be used to predict tsunami inundation on land. We used the dispersive tsunami model to simulate the 2011 Tohoku earthquake on the Supercomputer K. Good agreement was apparent between the dispersive wave model results and the tsunami waveforms observed offshore. The finest bathymetric grid interval was 2/9 arcsec (approx. 5 m) along longitude and latitude lines. Use of this grid simulated tsunami soliton fission near the Sendai coast. Incorporating the three-dimensional shape of buildings and structures led to improved modeling of tsunami inundation.

Key words: 2011 Tohoku tsunami, Boussinesq model, Dispersion, Soliton fission, Parallel computation.

1. Introduction

On 11 March 2011, a large, interplate earthquake between the Pacific and North American lithospheric plates occurred in the Japan Trench subduction zone. The Japan Meteorological Agency estimated the moment magnitude of the earthquake to be 9.0. The coastal region of eastern Japan was strongly shaken for 4–5 min, and that movement was followed by the devastating Tohoku tsunami. The tsunami completely destroyed many coastal cities along the eastern coast of Japan. Clear signals of the tsunami were recorded by tsunami gauges around the world during the event (Hayashi *et al.* 2011; Maeda *et al.* 2011). Many videos were also taken by evacuees and public agencies during the inundation of the coastal region. Tsunami height surveys were conducted at more than 5,900 points along the coast after the event (Mori *et al.* 2012).

Frequency dispersion is apparent in the far-field records of the 2011 Tohoku tsunami (Løvholt *et al.* 2012; Kirby *et al.* 2013). Dispersion of a tsunami occurs because water waves with different wavelengths travel at different speeds. Improvements in offshore tsunami observation technology have facilitated many observations of tsunami wave frequency dispersion in the open ocean in recent years (Horillo *et al.* 2006; Saito *et al.* 2010). Another remarkable phenomenon associated with tsunami dispersion occurred in the near-field region on the shallow, gentle slope along the Sendai coast. That phenomenon, called "tsunami soliton fission" (Shuto 1985), is characterized by split, short-period waves (or "undular bores") around the tsunami crest caused by a combination of wave nonlinearity and dispersion. The wave front of a tsunami propagating on a shallow, gentle slope becomes steep because of wave nonlinearity effects. When the wave front becomes sufficiently steep, the effect of wave dispersion begins to cause fission of the wave (Madsen *et al.* 2008). Analysis of a video of the Tohoku tsunami (Murashima *et al.* 2012) has

[1] Japan Agency for Marine-Earth Science and Technology (JAMSTEC), Yokohama Institute for Earth Sciences, 3173-25 Showa-machi, Kanazawa-ku, Yokohama, Kanagawa 236-0001, Japan. E-mail: baba.toshi@tokushima-u.ac.jp

[2] NEC Corporation, 5-7-1 Shiba, Minato-ward, Tokyo 108-8001, Japan.

[3] *Present Address*: Institute of Technology and Science, The University of Tokushima, 2-1 Minami-jyousanjima-cho, Tokushima 770-8506, Japan.

indicated that the wavelengths of the split waves ranged from 100 m to several hundred meters, and the amplitudes were several meters. If soliton fission occurs, the leading wave is amplified dramatically, the result being a larger tsunami force on coastal structures.

It is, therefore, essential to include the characteristics of tsunami soliton fission in tsunami modeling, but commonly used tsunami simulation models based on nonlinear and/or linear long-wave equations cannot reproduce tsunami soliton fission, because a tsunami soliton results from the combined effects of nonlinearity and dispersion. A Boussinesq-type approach that includes a dispersion term in the long-wave equations is an appropriate method for simulating tsunami soliton fission (Matsuyama *et al.* 2007, Murashima *et al.* 2010; Son *et al.* 2011; Zhou *et al.* 2011). Such simulation requires many computational resources. Rapid progress is being made, however, in parallel computing technology, an efficient way of solving the Boussinesq equations (Sitanggang and Lynett 2005).

In this study, we initially developed a new parallelized software by using message-passing interface (MPI) and open multi-processing (OpenMP) libraries; the software solves nonlinear Boussinesq-type dispersive equations with nested bathymetric grids. Sitanggang and Lynett (2005) constructed a parallelized scheme for Boussinesq modeling on a uniform finite-difference grid by domain decomposition. Zhou (2011) investigated a nested approach for Boussinesq modeling, but their approach did not include parallel technology. The software described in this paper enables parallel computation to be used simultaneously with a nesting algorithm. Implementation of this software enabled us to perform a large-scale dispersive tsunami modeling study with high spatial resolution and within a reasonable time. We then applied the new software to a modeling study of the 2011 Tohoku tsunami on the Supercomputer K, which at the time this paper was written was the fastest computer in Japan, and the fastest computer in the world from June 2011 to June 2012. The Supercomputer K is equipped with 82,944 computation processors for a total of 663,552 cores; it has achieved a Linpack performance of 10.51 petaflops with a high computing efficiency ratio of 93.2 % (Fujitsu 2012).

2. *Parallelized Dispersive Tsunami Software*

To perform large-scale dispersive tsunami wave modeling, we started with the URS Corporation and Geoscience Australia (URSGA) software provided by Jakeman *et al.* (2010). The numerical scheme used by URSGA is an explicit leapfrog difference method that solves either the linear or nonlinear long-wave equations in spherical coordinates. This scheme is based on the uniform finite-difference scheme of Satake (2002). Nonlinear terms in the model are approximated with upwind finite differences, and linear terms are approximated by two-point centered finite differences. The URSGA model uses a variable nested algorithm that enables the spatial resolution of the study region to be easily increased. The ratio of the grid spacing of the parent and child nested grids is 3:1.

Saito *et al.* (2010) reported a practical method for solving the linear Boussinesq equations derived from Peregrine (1972) with a uniform finite-difference scheme. By incorporating the method of Saito *et al.* (2010), we attempted to include the dispersion term in existing URSGA software. The URSGA software treats depth-averaged velocities (u and v) as dependent variables. Unfortunately, this software caused numerical instability during dispersive tsunami calculations in areas where the topography changed suddenly, for example at a continental shelf or trench axis. Conserved variables, however, have the property of being able to resolve discontinuities. Roeber *et al.* (2010) have described the transformation of physical to conserved variables in the Boussinesq equations. We therefore used conserved, depth-integrated variables to ensure stability during computation. This modification worked successfully and enabled us to avoid numerical instability during dispersive modeling. The governing equations used in the new software are expressed as:

$$\begin{aligned}\frac{\partial M}{\partial t}+\frac{1}{R\ \sin\theta}\frac{\partial}{\partial\varphi}\left(\frac{M^2}{d+h}\right)+\frac{1}{R}\frac{\partial}{\partial\theta}\left(\frac{MN}{d+h}\right)&\\ =-\frac{g(d+h)}{R\ \sin\theta}\frac{\partial h}{\partial\varphi}-fN&\\ -\frac{gn^2}{(d+h)^{7/3}}M\sqrt{M^2+N^2}&\\ +\frac{d^2}{3R\ \sin\theta}\frac{\partial}{\partial\varphi}\left[\frac{1}{R\ \sin\theta}\left(\frac{\partial^2 M}{\partial\varphi\partial t}+\frac{\partial^2(N\ \sin\theta)}{\partial\theta\partial t}\right)\right]&\end{aligned} \quad (1)$$

$$\frac{\partial N}{\partial t}+\frac{1}{R\ \sin\theta}\frac{\partial}{\partial\varphi}\left(\frac{MN}{d+h}\right)+\frac{1}{R}\frac{\partial}{\partial\theta}\left(\frac{N^2}{d+h}\right)$$
$$=-\frac{g(d+h)}{R}\frac{\partial h}{\partial\theta}+fM$$
$$-\frac{gn^2}{(d+h)^{7/3}}N\sqrt{M^2+N^2}$$
$$+\frac{d^2}{3R}\frac{\partial}{\partial\theta}\left[\frac{1}{R\ \sin\theta}\left(\frac{\partial^2 M}{\partial\varphi\partial t}+\frac{\partial^2(N\ \sin\theta)}{\partial\theta\partial t}\right)\right] \quad (2)$$

$$\frac{\partial h}{\partial t}=-\frac{1}{R\ \sin\theta}\left[\left(\frac{\partial M}{\partial\varphi}+\frac{\partial(N\ \sin\theta)}{\partial\theta}\right)\right] \quad (3)$$

where h is the water height from the sea surface at rest, t is time, φ and θ are the longitude and co-latitude, respectively, R is the earth's radius, d is the water depth, and the variables M and N are depth-integrated quantities equal to $(d+h)u$ and $(d+h)v$, respectively, along longitude and latitude lines, respectively. g is the gravitational constant, f is the Coriolis parameter, and n is Manning's roughness coefficient. In calculation of the dispersion terms [the final terms on the right-hand sides of Eqs. (1) and (2)], the fact that we used the static water depth (d) means that we ignored the dispersion effect on land to avoid risk of numerical instability caused by complex propagation during inundation. To solve these equations, we used the leapfrog, staggered-grid, finite-difference calculation scheme shown in the Appendix.

We used a domain decomposition method for parallel implementation of the Boussinesq model. We divided the finite-difference grid points of the nested grid into multiple rectangular sub-domains, each of the same size, the number of sub-domains being equal to the number of computation nodes (Fig. 1). An important aspect of decomposing the domain is load balancing. All computation nodes must have equal or almost equal amounts of data to be processed. This condition was achieved in the software by dividing all of the nested grids into the same number of sub-domains. Each sub-domain of the nested grids was associated with one computation node. For example, computation node No. 1 computed the No. 1 sub-domain of nested grid A, which was followed by computation of the No. 1 sub-domain of nested grid B, which was then followed by computation of the No. 1 sub-domain of nested grid C, and so forth. Multi-thread processing with OpenMP was also incorporated into the software for acceleration of loop calculations in the sub-domains. To calculate the variables h, M, and N in Eqs. (1)–(3) at a grid point, we must refer to data at the surrounding grid points. The data needed to calculate the variables at the edges of the sub-domains were acquired from the adjoining sub-domains. This data exchanges between the sub-domains were parallelized by the MPI point-to-point communication routines. To facilitate communication between the nested grids, data at the edges of a child nested grid were over-written by interpolated data from the parent nested grid. All of the data of the child nested grid were re-sampled to match the resolution of the parent nested grid, to enable copying of them to the parent nested grid (Fig. 2). This two-way inter-grid communication enabled seamless propagation of the tsunami between the nested grids. The inter-grid communications were implemented by using the MPI collective communication routines. Figure 3 shows a flowchart of the parallel dispersive computation with the nesting algorithm. We call the new parallelized software JAGURS-D, which stands for the Japan Agency for Marine-Earth Science and Technology (JAMSTEC) improvements of the URSGA software for dispersive tsunamis.

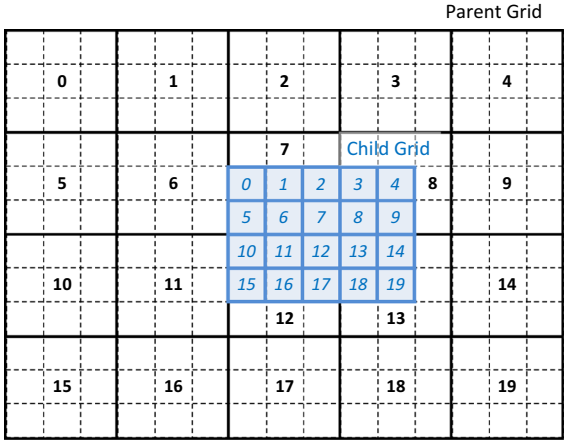

Figure 1
Nested gridding scheme and domain decomposition for parallel computation. *Numbers* indicate MPI ranks assigned for calculation of *rectangular sub-domains*

3. Tsunami Model Validation and Parallel Performance

For the purpose of validation of the dispersive tsunami model developed in this study, we used

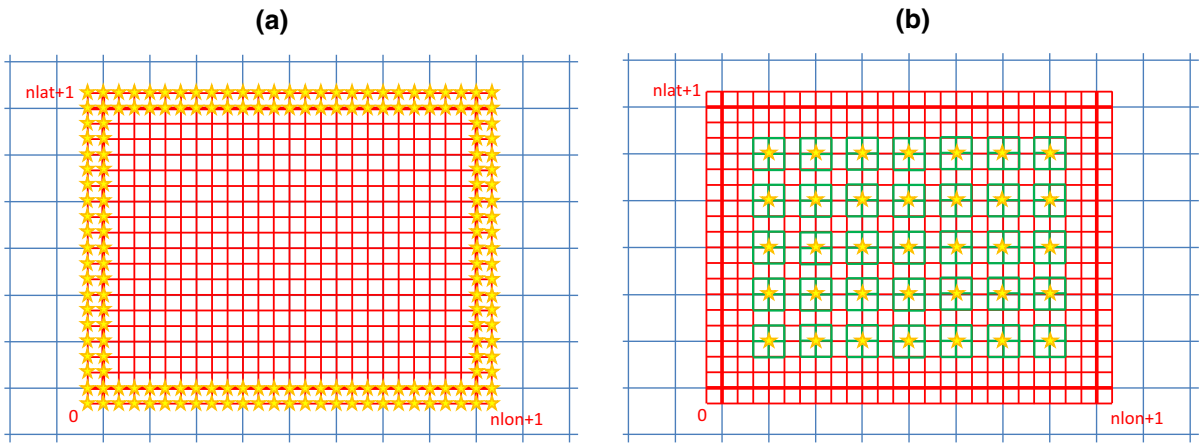

Figure 2
Inter-grid communications **a** from parent to child grids and **b** from child to parent grids. *Blue and red lines* indicate parent and child grid cells, respectively. The *stars* are points for transferred data. For data transfer from the parent to child, the data along the edges of the child grid were linearly interpolated by using the parent data, and copied to the child grid. For data transfer from the child to parent grids, we took an average of nine points of the child data, indicated by *green* in (**b**), to match the resolution of the parent grid

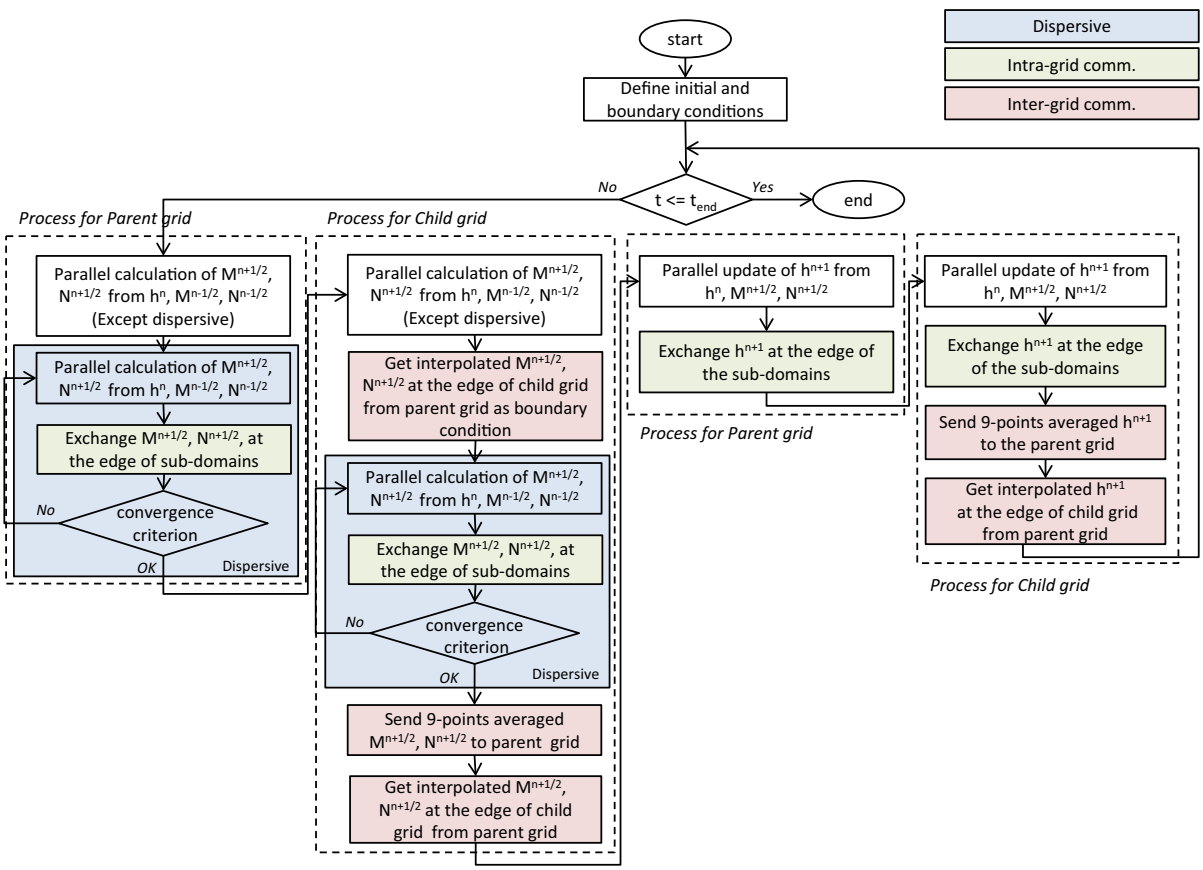

Figure 3
Flowchart of parallel dispersive tsunami calculation with the nesting algorithm. This example uses two nesting grids, parent and child grids, similar to the scheme shown in Fig. 1

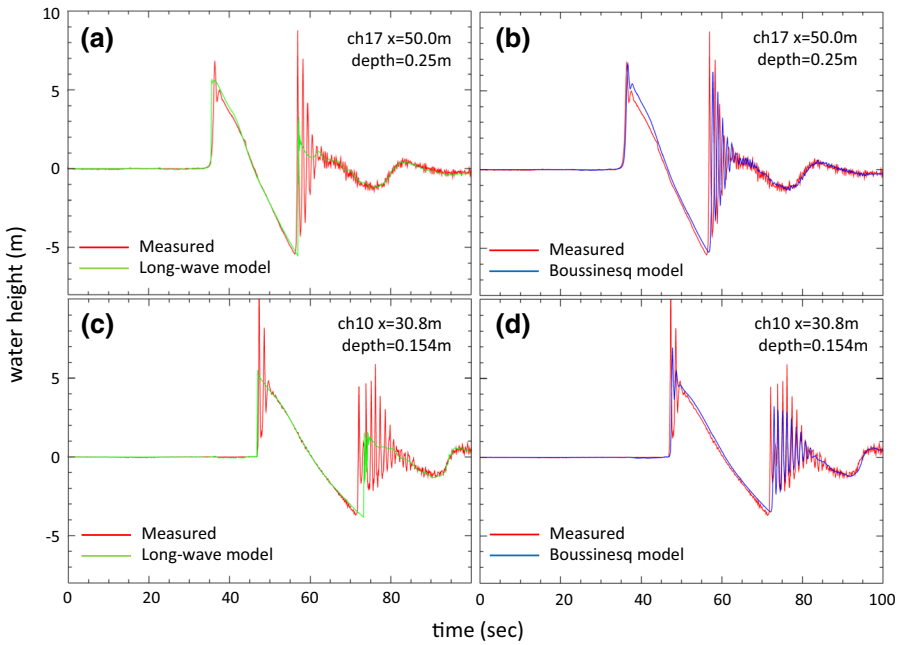

Figure 4
Time histories of water surface elevation calculated with the Boussinesq (*blue*) and long-wave (*green*) models compared with actual fluctuations (*red*) recorded in the wave flume experiment of MATSUYAMA *et al.* (2007)

results from MATSUYAMA *et al.* (2007). They conducted a large wave flume experiment to investigate the nature of tsunami soliton fission. The wave flume was 205 m long, 3.4 m wide, and had a maximum depth of 4.0 m (Figs. 1, 2 in MATSUYAMA *et al.* 2007). We used water surface waveforms recorded during the experiment for which the input wave period was 20 s and the wave amplitude was 0.03 m on a slope gradient of 1/200 (Fig. 5 in MATSUYAMA *et al.* 2007). Soliton fission occurred at a point 50 m from the modeled shoreline (wet and dry boundary) in that experiment. We constructed a topographic model that simulated the wave flume topography from distances of 80 m to −10 m from the modeled shoreline, with a grid interval of 0.1 m. We have given the recorded waveform time series at a point 80 m from the modeled shoreline as the boundary condition in the calculation. It should be noted that we modified the software from spherical coordinates to Cartesian coordinates to avoid cancellation of significant digits. A single topographic grid with no nesting was applied with a time step of 0.005 s and a Manning's coefficient of 0.025. The integral time was set to 300 s.

Figure 4 shows a comparison of measured (MATSUYAMA *et al.* 2007) and calculated waveforms at two points 50.0 and 30.8 m from the modeled shoreline in the wave flume experiment. The conventional nonlinear long-wave model (Fig. 4a, c) predicted the timing of tsunami arrival and the characteristics of the waveform, except for the soliton fission waves. It could not, however, predict any component of the soliton fission wave. After the wave front became steep, because of nonlinear effects, the wave front propagated without fission in the long-wave model. In contrast, the Boussinesq model developed in this study (Fig. 4b, d) simulated well the time histories of water surface fluctuations recorded in the wave flume experiment, including the soliton fission wave. We can therefore assert that our dispersive tsunami model can be used to investigate issues related to tsunami soliton fission phenomena.

Next, we verified correct operation of the nesting algorithm. We simulated the tsunami caused by the 2011 Tohoku earthquake, using the dispersive model with five nested grids shown in Fig. 5. The finest nesting grid was located on the Sendai coast, where soliton fission was observed during the 2011 Tohoku tsunami. This grid was divided into grid points separated by approximately 2/9 arcsec (about 5 m). The total number of grid points was 21 million. The

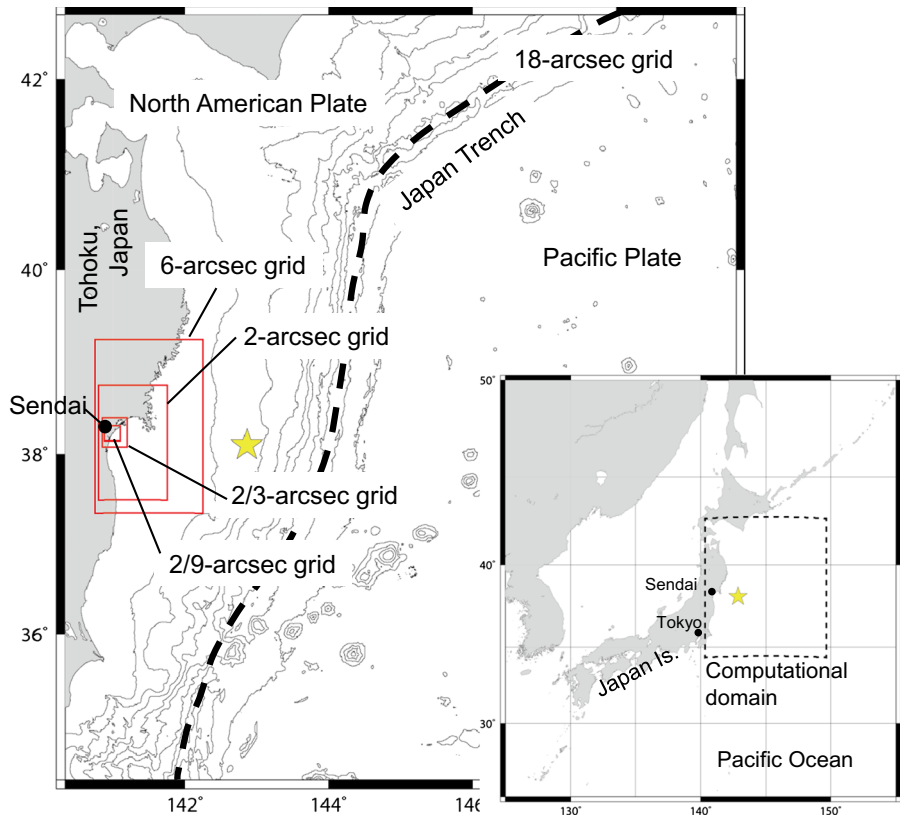

Figure 5
Bathymetry of the computational domain (18-arcsec grid spacing) and *outlines* of nested grids (*rectangles outlined in red*). The depth contour interval is 1,000 m. The *dashed line* is the axis of the Japan Trench. The *star* indicates the epicenter of the 2011 Tohoku earthquake determined by the Japan Meteorological Agency

time step was set to 0.1 s to satisfy the stability condition.

Figure 6 is a sequential time series of maps that indicate sea surface height around the boundary of the nesting grids. Analysis of these maps revealed that the calculated tsunami propagated seamlessly beyond the boundaries of the nesting grids. This result means that the algorithm implemented with our software can successfully achieve transfer of variables between the nesting grids needed to solve the dispersive equations under the parallelized computational scheme.

We also performed a parallel performance test of JAGURS-D on the K computer using the set up described above. We used the MPI+OpenMP mixed parallel model with automatic parallelization by the compiler. We repeated the calculations by changing number of nodes (12, 24, 48, 96, and 192) and measured elapsed time. One node of the K computer consists of eight processing cores. Figure 7 shows the acceleration ratio achieved in the test. Addition of up to 192 nodes efficiently upgraded the speed of computation.

4. Simulation Model for the 2011 Tohoku Tsunami

Many source models have been suggested for the 2011 Tohoku earthquakes, on the basis of seismic data (Ammon *et al.* 2011; Yagi and Fukahata 2011), tsunami data (Imamura *et al.* 2011; Saito *et al.* 2011; Satake *et al.* 2013), and crustal deformation data (Suito *et al.* 2011; Ito *et al.* 2011). Goto *et al.* (2012) and Baba *et al.* (2014) used the tsunami source model proposed by Imamura *et al.* (2011) for simulation of the near-field tsunami. Grilli *et al.* (2013) simulated two forms of the Tohoku tsunami derived from a source inverted from teleseismic waves (Shao *et al.*

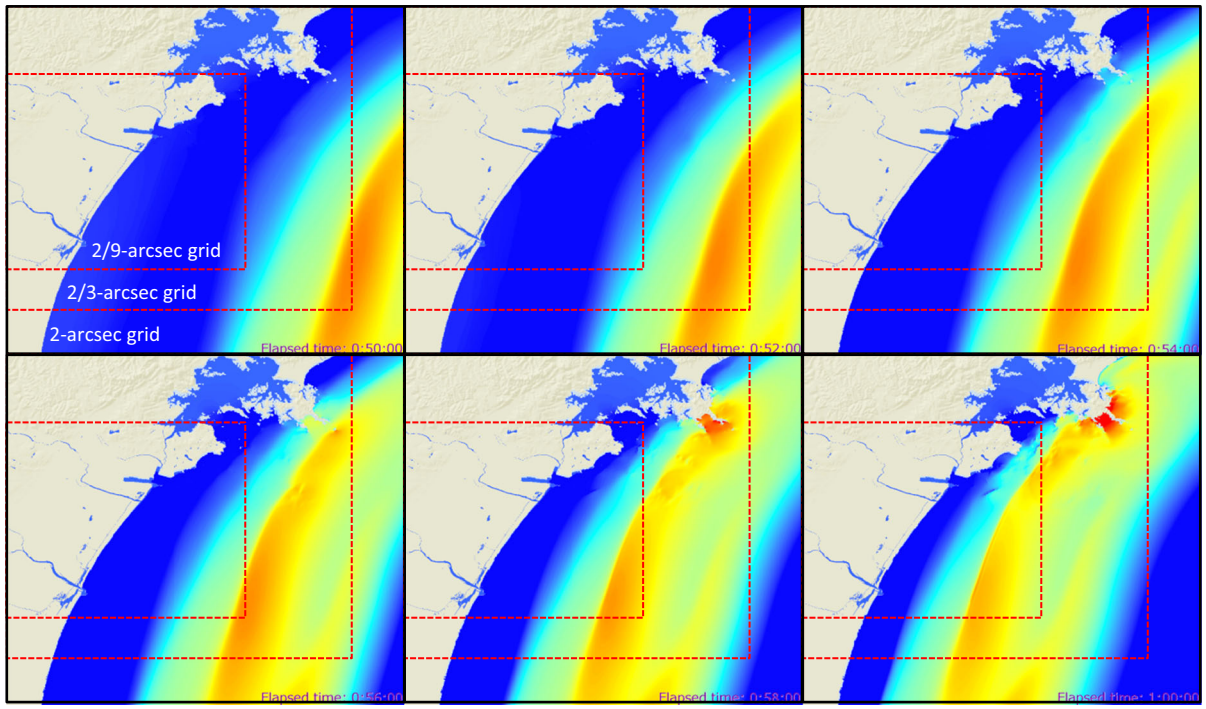

Figure 6
Successive views of water surface elevation during the 2011 Tohoku tsunami, near the Sendai coast, calculated by use of the dispersive tsunami software. *Red dotted lines* indicate the boundaries of nesting grids. The calculated tsunami propagated seamlessly beyond the nesting boundaries

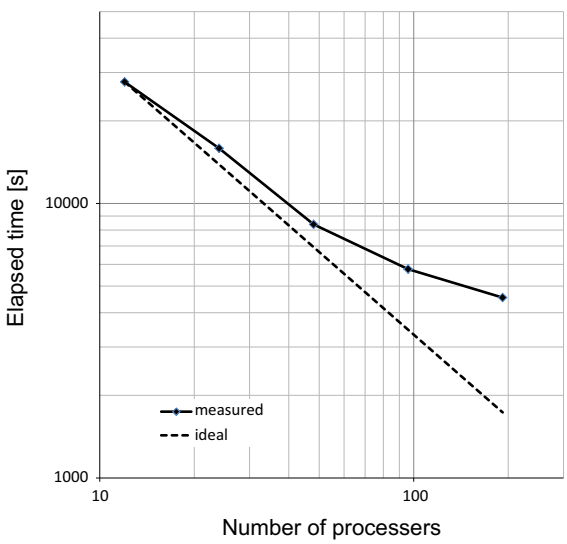

Figure 7
Parallel performance test of JAGURS on the K computer

2011) and their own source based on geodetic data, including sea floor displacements. We used the 2011 Tohoku tsunami source obtained by SAITO *et al.* (2011) in this study, because it is the only model derived from linear dispersive tsunami equations. They inverted the observed tsunami waveforms for the 2011 tsunami source with dispersive Green's functions calculated in a uniform finite-difference scheme. In general, we did not use the dispersive equations but, instead, used linear long-wave equations in tsunami inversion analysis on the assumption that dispersion effects are negligible in the near-field. This assumption is valid when the wavelength of the tsunami source is long enough to be comparable with the water depth. However, the offshore tsunami gauges recorded very short-wavelength tsunami waves during the 2011 tsunami. In this case, the linear long-wave equations could not correctly simulate the short-wavelength tsunami waves, the result being an incorrect image of the tsunami source after inversion analysis. Accordingly, we selected the Saito's model derived from dispersive Green's functions to implement the dispersive tsunami modeling.

For modeling of the 2011 Tohoku tsunami, five bathymetric nested grids, shown in Fig. 5, were

defined for our calculation. The coarsest grid represented the entire computational domain (34–43°N, 140–150°E), including the tsunami source and the target area of Sendai (Fig. 5). The bathymetry in the grid was obtained by use of a combination of the M7000 map series provided by the Marine Information Research Center, Japan Hydrographic Association, the Tohoku bathymetric grid from JAMSTEC (KIDO *et al.* 2011), and General Bathymetric Chart of the Oceans (GEBCO) data (British Oceanographic Data Centre 2010). The bathymetry was interpolated to 18 arcsec intervals. The M7000 series is a set of digital bathymetric contours obtained by combining the basic maps of the coastal waters of Japan with other bathymetric information. The Tohoku bathymetric grid includes all results from JAMSTEC's multi-narrow beam surveys conducted in the Japan Trench. GEBCO provides global bathymetry datasets for the world's oceans with spatial resolution of 30 arcsec. These datasets were subsampled and then interpolated to make nested grids with spacings of 6, 2, 2/3, and 2/9 arcsec for the nesting scheme.

For the land area, we re-sampled Geospatial Information Authority of Japan (GSI) data to produce topographic grids. The 50-m-interval topographic data assembled by the GSI, which covers all of Japan, were used for the topography in grids with spacing of 18, 6, and 2 arcsec. The 5-m interval topographic data provided by the GSI were re-sampled and interpolated to 2/3 and 2/9 arcsec grids. These topographic grids were merged with the bathymetric grids to yield seamless bathymetric–topographic grids for the entire region. The shape of the coastline, which is important in tsunami modeling, was based on GSI topographic data. The shapes of tsunami defense facilities, for example sea walls and breakwaters larger than 7.5 m, were included as topography in the finest digital elevation model (DEM) data. The tide level was approximately −25 cm when the tsunami arrived at the coast in the finest grid (gridded by 2/9 arcsec spacing). We imitated the tide level by relative uplifting of the ground by 25 cm in the simulation. To consider the crustal deformation as a result of the faulting of the 2011 Tohoku earthquake, we again lowered the ground level in the 2/9 arcsec grid by 35 cm, on the basis of NISHIMURA *et al.* (2011).

We performed a nonlinear dispersive simulation of the tsunami generated by the 2011 Tohoku earthquake by use of the dataset described above. A sponge buffer zone (CERJAN *et al.* 1985) was applied

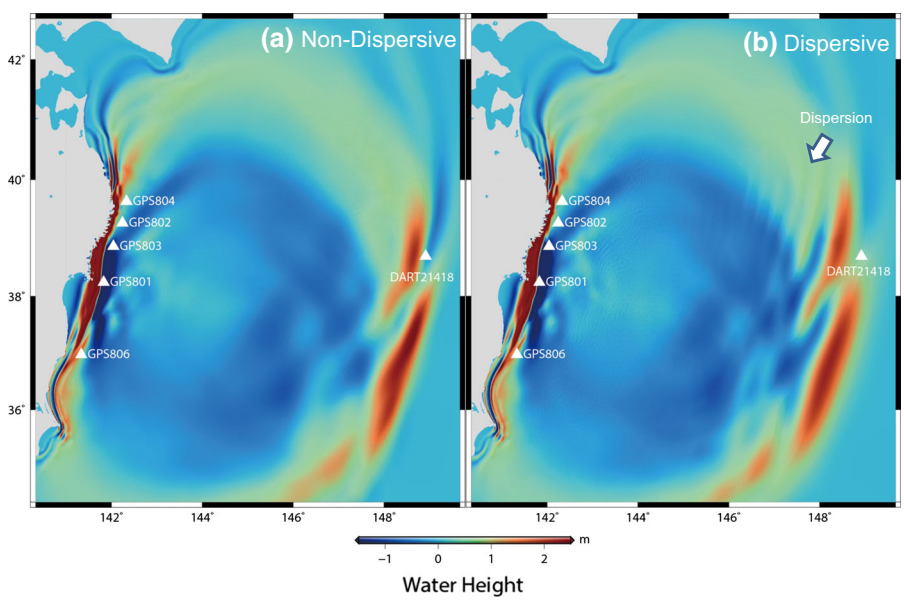

Figure 8
Sea-surface fluctuations 30 min after the earthquake occurred, simulated with nonlinear long-wave equations (**a**) and nonlinear dispersive wave equations (**b**). *Triangles* indicate locations of tsunami gauges. Tsunami waveforms are compared in Fig. 9

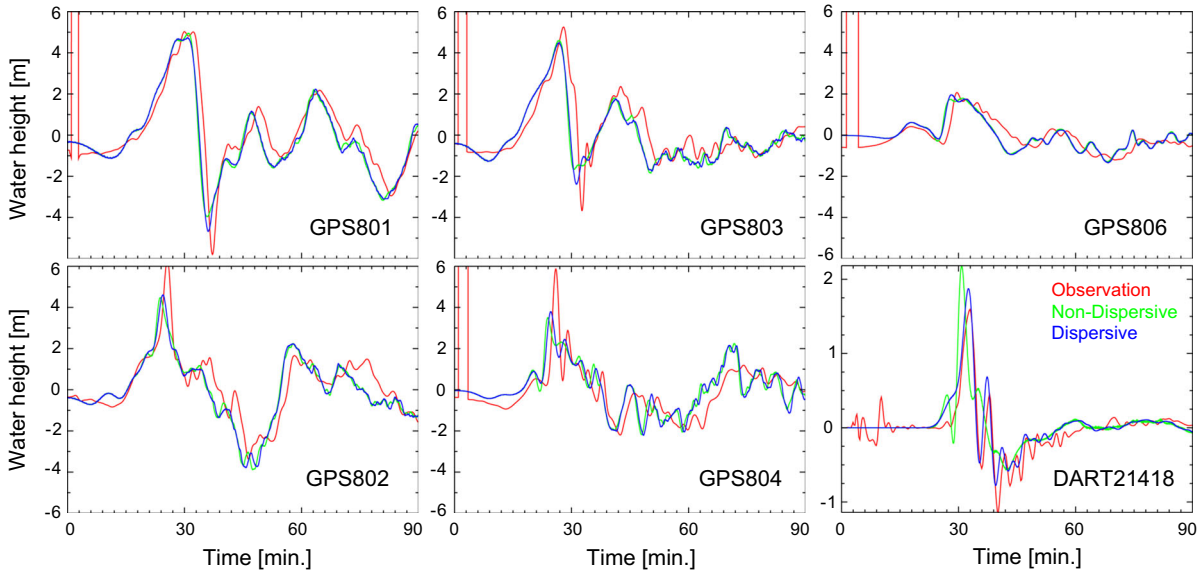

Figure 9
Comparisons of tsunami waveforms determined from observations (*red*), the non-dispersive model (*green*), and the dispersive model (*blue*) at the offshore stations. The locations of the stations are shown in Fig. 8. *Horizontal axis* is elapsed time after the 2011 Tohoku earthquake. The records from stations *GPS801*, *GPS803*, *GPS806*, and *GPS804* lack data at the beginning

at the 60 grid points surrounding the simulation model to avoid reflection of short-period tsunami waves at the outer boundary of the calculation region. For the sea–land boundary, we used a moving boundary so that the tsunami could inundate the land. A uniform Manning's coefficient of 0.025 s $m^{-1/3}$ was used for the whole computation region. The time step was set to be 0.1 s, to satisfy the stability condition for the finite difference algorithm. The integral time was 3 h, including the arrival time of the major tsunami waves at the target region. We implemented this calculation on 192 nodes (1,536 cores) of the K computer. The computation results were produced after an elapsed time of approximately 9.5 h. Non-dispersive modeling, based on the nonlinear long-wave equations, was also performed for comparison.

5. Results and Discussion

Ocean-bottom pressure gauges and global positioning system (GPS) buoys around Japan successfully documented the 2011 Tohoku tsunami offshore (Maeda *et al.* 2011; Hayashi *et al.* 2011). These offshore gauges were able to provide tsunami waveforms free from such complicating effects as nonlinearity, reflection, and refraction near the coast. These data were therefore useful for validating our dispersive tsunami simulation. Figure 8 compares sea-surface fluctuations between the long-wave and dispersive models. In the region near buoy DART21418, frequency dispersion was apparent in the dispersive simulation (arrow in Fig. 8). Simulated and observed tsunami waveforms are compared in Fig. 9. In the case of the tsunami waveform observed at DART21418, the first tsunami wave was followed by several short-period waves during the time interval from 30 to 60 min after the time of origin of the earthquake. The dispersive simulation produced similar results. This similarity reflects the fact that the source model of Saito *et al.* (2011) used dispersive tsunami equations and was adjusted to reproduce the observed data at buoy DART21418. The point is that the short-period wave train following the first tsunami appeared only in the dispersive simulation, but not in the non-dispersive simulation. In contrast, the discrepancy between the non-dispersive and dispersive models was not apparent in the tsunami waveforms recorded by GPS buoys near the Japanese coast. This information is important for determining whether dispersive or non-dispersive

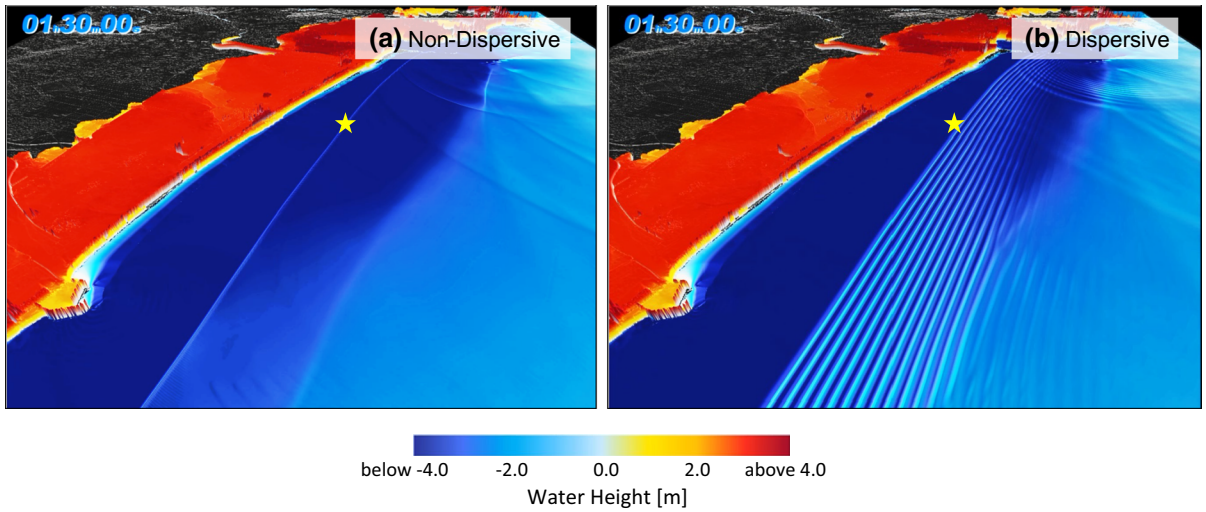

Figure 10
Sea-surface fluctuations of the 2/9-arcsec grid near the Sendai coast 90 min after the earthquake occurred, simulated by use of nonlinear long-wave equations (**a**) and the nonlinear dispersive wave equations (**b**). The *star* indicates the location of the waveform of sea-surface fluctuations plotted in Fig. 11

equations should be used to create Green's functions for source inversion analysis with the tsunami waveforms.

These two models provided quite different images of the area very close to the Sendai coast (Fig. 10). The dispersive model successfully predicted the occurrence of tsunami soliton fission approximately 90 min after the earthquake, when the second large tsunami wave was approaching the coast. The computed wavelength of each split wave was approximately 200 m. Figure 11 shows a comparison of the non-dispersive and dispersive simulations of the tsunami waveforms near the coast. We were able to count 13 split waves in the tsunami waveforms obtained with the dispersive model. The maximum peak-to-trough amplitude of the soliton fission was approximately 3 m. The period of that wave was approximately 13 s. These features of the soliton fission waves were consistent with reports from helicopter observations (MURASHIMA *et al.* 2010). This dispersive model, which used a fine topographic grid interval of 0.22 arcsec (approx. 5 m), simulated the soliton fission waves of the 2011 Tohoku tsunami quantitatively near the coast. We stress that dispersive modeling is essential for simulating the characteristic tsunami phenomena near a coast and the frequency dispersion often observed in the open ocean.

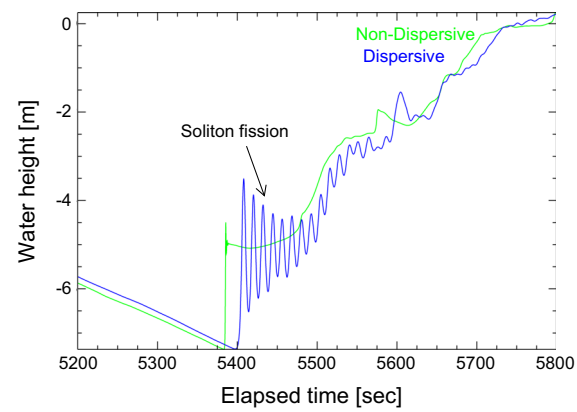

Figure 11
Tsunami waveforms derived from non-dispersive (*green*) and dispersive (*blue*) models at the point indicated by the *star* in Fig. 10

We mapped the differences between the simulated maximum tsunami height in the two models (Fig. 12). Although we were able to describe the tsunami soliton fission for the second tsunami wave as described above, the maximum tsunami height was produced during the first tsunami wave, when the soliton fission wave was less apparent in the calculation. However, weak soliton fission occurred at a point very close to the coast for the first tsunami wave. The occurrence of this soliton fission was accompanied by a large-amplitude tsunami wave near

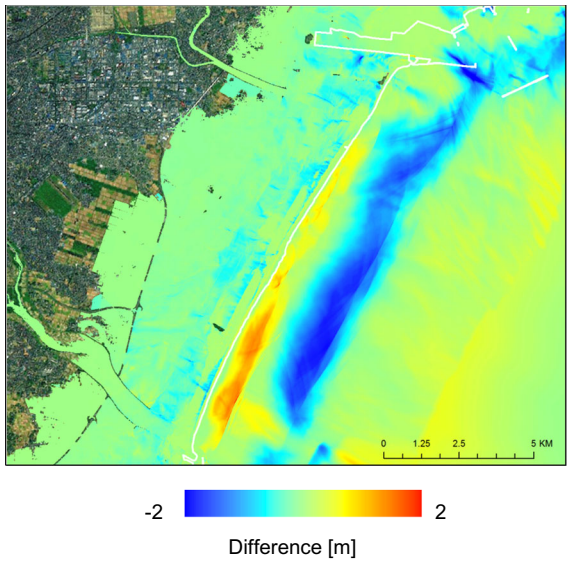

Figure 12
Difference between maximum tsunami height in the non-dispersive and dispersive models for the 2/9-arcsec grid. *Positive values* indicate greater height simulated by the dispersive model. The *white line* is the coastline

the coast. This fact is apparent in Fig. 12, which depicts the difference between the simulated maximum height of the tsunami in the dispersive and non-dispersive models. A positive (greater height in the dispersive model) band of approximately 1 m is apparent along the coastline. In contrast, a negative (smaller height in the dispersive model) band is apparent offshore of the positive band. The amplitude of the nonlinear long-wave tsunami becomes large because of the shoaling effect as the wave approaches the coast. The dispersion term also works to depress the amplification because of wave nonlinearity. Consequently, the dispersive model may produce a tsunami of smaller amplitude than the nonlinear long-wave model when soliton fission does not occur.

How does the dispersive model make a difference in terms of tsunami inundation on land? Comparison of the calculated results revealed that the dispersive model resulted in maximum inundation slightly smaller than the long-wave model (Fig. 12). But the countermeasures taken against a tsunami disaster would make the difference negligible. This small difference may be related to the fact that the maximum inundation was recorded during the first tsunami wave, when soliton fission was much less apparent than it was during the second wave. We therefore do not believe the tsunami derived from the dispersive simulation to produce the maximum inundation on land differs from that of the long-wave model. A previous study that investigated the effect of using a dispersive model to simulate inundation during the 2004 Sumatra tsunami (Shigihara *et al.* 2006) revealed that the dispersive model and long-wave models produced similar inundation results. However, for the 1983 Nihonkai-Chubu earthquake, a dispersive model resulted in a much larger inundation (Iwase 2005). It would be inappropriate to conclude how much use of a dispersive model affects the simulated inundation. The effect may differ on case-by-case basis. With the dataset we used, inclusion of dispersion in the model had little effect on the maximum simulated inundation height on land.

In this study, we used a source model inverted from only offshore tsunami waveforms observed by ocean-bottom pressure gauges and GPS buoys (Imamura *et al.* 2011). These offshore tsunami gauges are able to detect a tsunami before it arrives on the coast and are therefore useful for early prediction of tsunami. In fact, several algorithms for estimating the source of a tsunami on a real-time basis have been investigated by inverting offshore data (Tsushima *et al.* 2012; Takagawa and Tomita 2012). Our concern is how accurately the characterization of a tsunami source based on inversion of offshore tsunami data describes the tsunami and inundation near the coast with the methodology used in this study. Mori (2011) measured numerous tsunami inundation heights in the coastal region after the 2011 Tohoku tsunami. Our simulation results are compared with their survey results in Fig. 13. The predicted and observed tsunami heights are positively correlated (Fig. 13c). We also used Aida's method (Aida 1978) to quantitatively validate the numerical simulation. Aida (1978) defined two indices, the geometric mean K and geometric standard deviation κ, that can be used to evaluate the reproducibility of numerical simulations of tsunami events. For the data in Fig. 13, the calculated K and κ values were 0.94 and 1.28, respectively.

However, this model seems to systematically underestimate tsunami heights along the coastline (Fig. 13b). We took into account highly accurate DEM data in the tsunami simulation, but large, strong

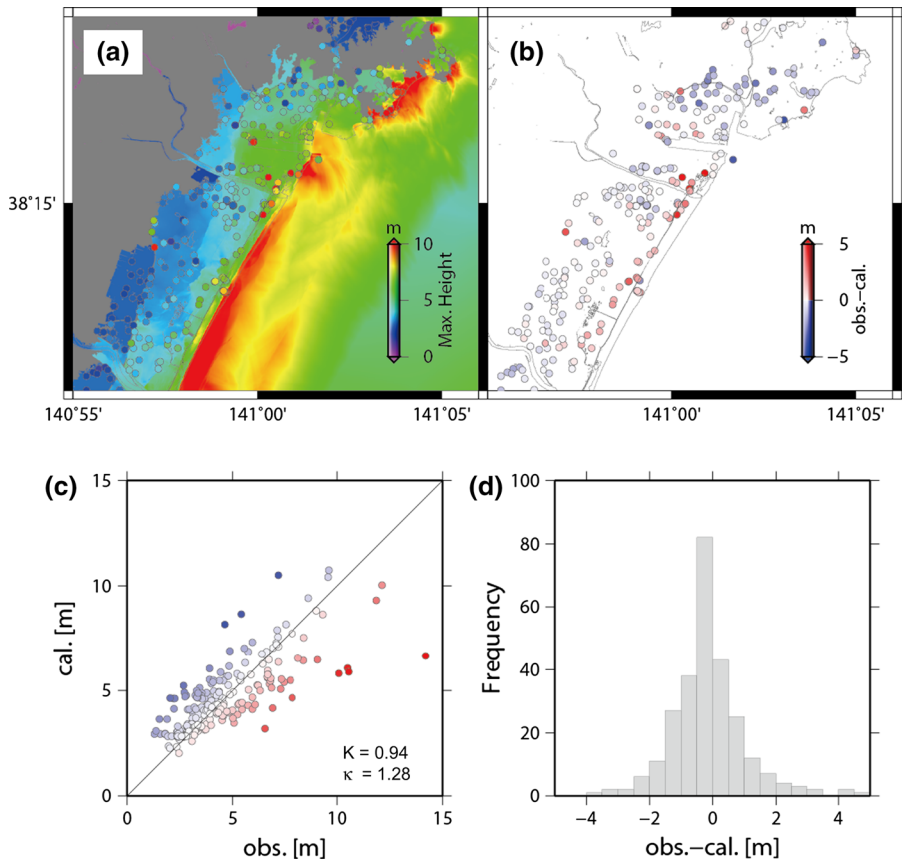

Figure 13
Comparison of measured inundation heights and simulations with the dispersive model using conventional DEM. **a** *Colored map* showing the maximum inundation height in the 2/9-arcsec grid obtained with the simulation. *Colored circles* are derived from a field survey (Mori 2011). **b** The map shows differences between observed and calculated heights at specific points. **c** Relationship between observed and calculated values. The *straight line* indicates equality of calculated and observed values. K and κ are the geometric mean and geometric standard deviation, respectively, of the reproduction indices, proposed by Aida (1978). **d** Histogram of deviations of the calculated values from the observations

buildings should, similar to sea walls, afford direct protection against an incoming tsunami. We inferred that incorporating three-dimensional (3D) shapes of buildings and structures may lead to improved modeling of tsunami inundation in the coastal region. Lidar measurements are being carried out along the Japanese coast by the GSI. Lidar collects reflections with high spatial resolution from the ground surface, and reflections from such elevated surfaces as roads, bridges, the roofs of buildings, and the tops of trees. We therefore embedded the 3D building data derived from lidar measurements as topographic highs in the dispersive tsunami model to reproduce tsunami barriers in the coastal area. We repeated the tsunami calculation after replacing topographic data from the DEM only with data that included 3D building information embedded in the DEM (Fig. 14). The predicted tsunami became large in front of the buildings along the coastline. The predicted maximum inundations reproduced observations better than the maximum inundations obtained with the DEM model. The values of K and κ were improved to 0.97 and 1.27, respectively. These values satisfy the adequacy criteria for tsunami numerical modeling established by the Japan Society of Civil Engineers (2002) ($0.95 < K < 1.05$, $\kappa < 1.45$). The 3D building data helped to improve the accuracy of the simulated inundations. We conclude that the measured heights were simulated well by this method of calculation, which used 3D building data and tsunami source information acquired with

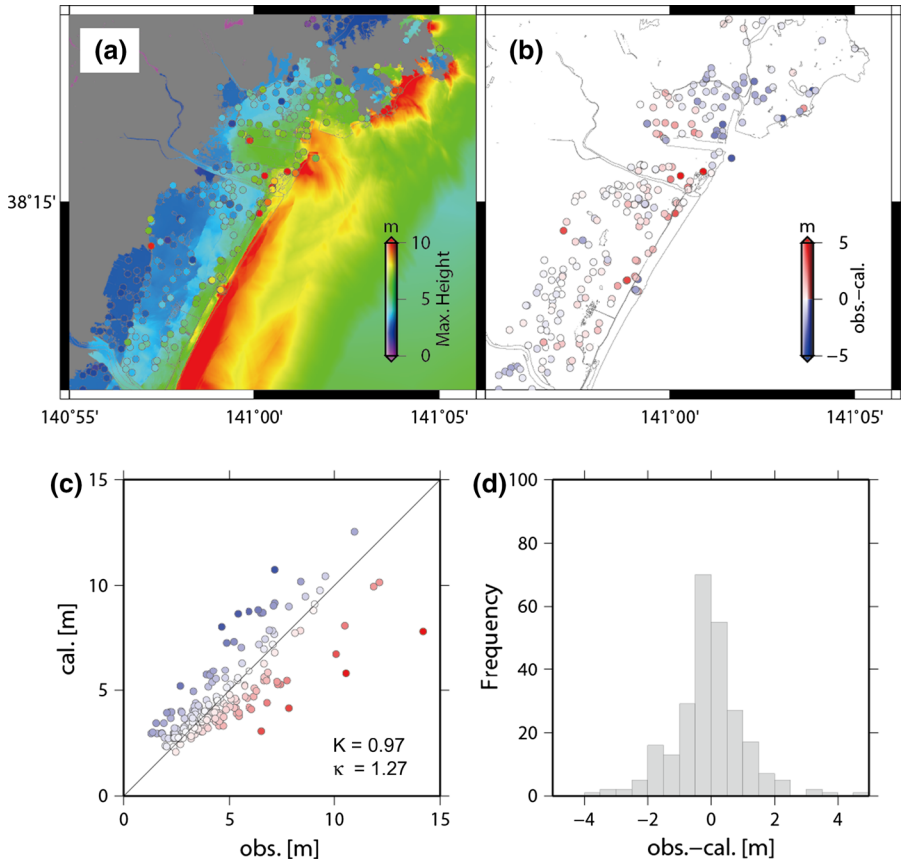

Figure 14
Comparison of measured inundation heights and simulations with the dispersive model using three-dimensional shapes of buildings embedded in the DEM. The *panels* are explained in the caption to Fig. 13

offshore data only without the coastal data. In this study, we successfully developed high-speed software for tsunami propagation and inundation. It would now be very desirable to develop a practical and real-time method that can accurately characterize tsunami sources by analysis of offshore tsunami data for mitigation of future tsunami damage.

During the tsunami simulations, we developed two ideas for further improving the accuracy of tsunami models. The first idea relates to topographic data. We applied the highly accurate DEM and 3D building data on land, and used highly reliable data for the shape of the sea bottom. There were, however, no measured data for such inland waters as rivers, ponds, and small channels, so topographic shape was generated by interpolating surrounding data. The reproducibility of the observed tsunami height was relatively poor in these areas in this simulation. The second idea concerns the finite-difference scheme in the current software. The current model uses a low-order upwind differencing method to calculate the nonlinear term, but that method is associated with significant numerical dissipation when the flow curvature is large (MATSUYAMA *et al.* 2010; SON *et al.* 2011). The result may be an obstructive factor that prevents amplification of the height of the tsunami because of nonlinear and dispersion effects. We are attempting to solve these problems so the model can predict tsunami characteristics more accurately with high speed and high resolution.

6. Conclusions

In this study we developed new software for dispersive tsunami wave modeling. The software solves

the nonlinear Boussinesq dispersive equations in a finite-difference scheme with variable nested grids. The software was fully parallelized with the MPI and OpenMP libraries so that large-scale dispersive modeling of the 2011 Tohoku tsunami was possible on the K Supercomputer. A clear discrepancy was apparent from comparison of tsunami waveforms derived from dispersive and non-dispersive simulations at the DART21418 buoy located in the deep ocean. Tsunami soliton fission near the coast recorded by helicopter observations was accurately reproduced by the dispersive model with the high-resolution grids. This calculation scheme, with incorporation of 3D data on building shapes and tsunami source characteristics independently retrieved from offshore data alone, satisfied the adequacy criteria for the prediction of tsunami traces on land.

Acknowledgments

Dr Hong Kie Thio, Dr Phil Cummins, and Dr David Burbidge kindly provided us with the URSGA tsunami software. The wave flume experimental data was provided by the Central Research Institute of the Electric Power Industry. The 2011 Tohoku tsunami data for the GPS buoy were provided by the Ministry of Land, Infrastructure, Transport and Tourism, and DART data came from the Pacific Marine Environmental Laboratory. The DEM and 3D building data were provided by the Geospatial Information Authority of Japan. The digital data of the initial sea-surface displacement of the 2011 Tohoku tsunami were provided by Dr Tatsuhiko Saito. Comments from Dr Takayuki Miyoshi and Dr Takane Hori were very useful for improving the manuscript. We thank anonymous reviewers for constructive comments. This research was implemented in the Strategic Programs for Innovative Research, Field 3, and was also partially supported by the Science and Technology Research Partnership for Sustainable Development. Some figures were prepared by use of Generic Mapping Tools (Wessel and Smith 1998), Seismic Analysis Code (Goldstein *et al.* 2007), and ArcGIS.

Appendix: Finite-difference Scheme for Nonlinear Dispersive Equations

The finite difference calculation was performed in the staggered-grid system shown in Fig. 15. Because the integration over time was solved with a leapfrog method, the water height (h) was defined at time $t = n\Delta t$, and the depth-integrated quantities (M, N) were defined at $t = (n - 1/2)\Delta t$, where Δt is the time step and $n = 1, 2, 3\ldots$. In the Appendix, φ and θ indicate the longitude and co-latitude, respectively, R is the earth's radius, d is the water depth, and D is total depth, that is $d + h$. g is the gravitational constant, f is the Coriolis parameter, and n is the Manning's roughness coefficient. We considered the finite-difference form of the dispersion term, the final term on the right-hand side of Eq. (1).

$$\frac{d^2}{3R\ \sin\theta}\frac{\partial}{\partial\varphi}\left[\frac{1}{R\ \sin\theta}\left(\frac{\partial^2 M}{\partial\varphi\partial t}+\frac{\partial^2(N\ \sin\theta)}{\partial\theta\partial t}\right)\right] = \frac{d^2}{3R^2\sin^2\theta}\frac{\partial}{\partial t}\left(\frac{\partial^2 M}{\partial\varphi^2}+\frac{\partial^2(N\ \sin\theta)}{\partial\varphi\partial\theta}\right), \tag{4}$$

where

$$\frac{\partial^2 M}{\partial\varphi^2} = \frac{M_{i+1,j} - 2M_{i,j} + M_{i-1,j}}{\Delta\varphi^2}, \tag{5}$$

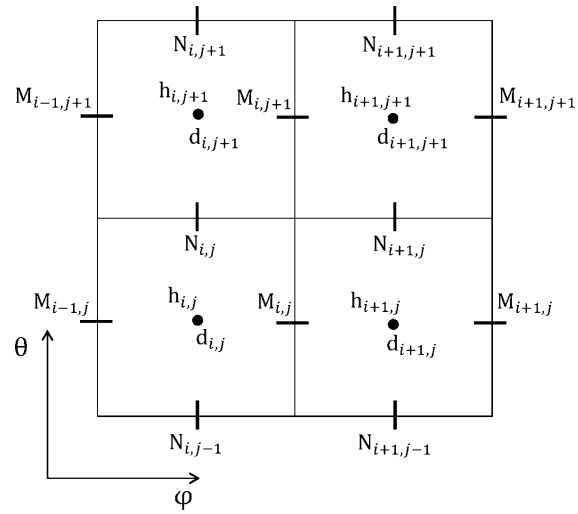

Figure 15
Staggered-grid system for the finite-difference simulation of nonlinear dispersive equations

$\Delta\varphi$ is the grid size along a longitude line. We introduced

$$U = M_{i+1,j} - 2M_{i,j} + M_{i-1,j}, \tag{6}$$

to write

$$\frac{\partial}{\partial t}\left(\frac{\partial^2 M}{\partial \varphi^2}\right) = \frac{\partial}{\partial t}\left(\frac{U}{\Delta\varphi^2}\right) = \frac{U^{n+\frac{1}{2}} - U^{n-\frac{1}{2}}}{\Delta\varphi^2 \Delta t}. \tag{7}$$

The other term of Eq. (4) can be expressed as:

$$\begin{aligned}\frac{\partial^2(N\ \sin\theta)}{\partial\varphi\partial\theta} &= \frac{\partial}{\partial\varphi}\left(\frac{\bar{N}_{i,j+1}\sin(\theta+\Delta\theta) - \bar{N}_{i,j}\sin(\theta)}{\Delta\theta}\right) \\ &= \frac{\bar{N}_{i,j+1}\sin(\theta+\Delta\theta) - \bar{N}_{i-1,j+1}\sin(\theta+\Delta\theta) - \bar{N}_{i,j}\sin(\theta) + \bar{N}_{i-1,j}\sin(\theta)}{\Delta\theta\Delta\varphi},\end{aligned} \tag{8}$$

where $\Delta\theta$ is the grid size along a latitude line. Because of the staggered grid system:

$$\bar{N}_{i,j} = \frac{N_{i,j} + N_{i+1,j} + N_{i,j-1} + N_{i+1,j-1}}{4}. \tag{9}$$

By defining:

$$\begin{aligned}\bar{V} = {} & \bar{N}_{i,j+1}\sin(\theta+\Delta\theta) - \bar{N}_{i-1,j+1}\sin(\theta+\Delta\theta) \\ & - \bar{N}_{i,j}\sin(\theta) + -\bar{N}_{i-1,j}\sin(\theta),\end{aligned} \tag{10}$$

we can write:

$$\frac{\partial}{\partial t}\left(\frac{\partial^2(N\ \sin\theta)}{\partial\varphi\partial\theta}\right) = \frac{\partial}{\partial t}\left(\frac{\bar{V}}{\Delta\theta\Delta\varphi}\right) = \frac{\bar{V}^{n+\frac{1}{2}} - \bar{V}^{n-\frac{1}{2}}}{\Delta\theta\Delta\varphi\Delta t}. \tag{11}$$

Accordingly, the dispersion term of Eq. (1) can be expressed by using Eqs. (7) and (11) in finite-difference form as:

$$\begin{aligned}&\frac{d^2}{3R\ \sin\theta}\frac{\partial}{\partial\varphi}\left[\frac{1}{R\ \sin\theta}\left(\frac{\partial^2 M}{\partial\varphi\partial t} + \frac{\partial^2(N\ \sin\theta)}{\partial\theta\partial t}\right)\right] \\ &\quad = \frac{\bar{d}_{i,j}^2}{3R^2\sin^2\theta\Delta t}\left(\frac{U^{n+\frac{1}{2}} - U^{n-\frac{1}{2}}}{\Delta\varphi^2} + \frac{\bar{V}^{n+\frac{1}{2}} - \bar{V}^{n-\frac{1}{2}}}{\Delta\theta\Delta\varphi}\right),\end{aligned} \tag{12}$$

where also, because of the staggered grid system:

$$\bar{d}_{i,j} = \frac{d_{i,j} + d_{i+1,j}}{2} \tag{13}$$

Finally, Eq. (1) can be written in finite-difference form as:

$$\begin{aligned}M^{n+\frac{1}{2}} = {} & M^{n-\frac{1}{2}} - \frac{1}{R\ \sin\theta}\frac{\Delta t}{\Delta\varphi}\left(\frac{M_{i+1,j}^{n-\frac{1}{2}2}}{\bar{\mathrm{D}}_{i+1,j}} - \frac{M_{i,j}^{n-\frac{1}{2}2}}{\bar{\mathrm{D}}_{i,j}}\right) \\ & - \frac{1}{R}\frac{\Delta t}{\Delta\theta}\left(\frac{M_{i,j+1}^{n-\frac{1}{2}}\bar{N}_{i,j+1}^{n-\frac{1}{2}}}{\bar{\mathrm{D}}_{i,j+1}} - \frac{M_{i,j}^{n-\frac{1}{2}}\bar{N}_{i,j}^{n-\frac{1}{2}}}{\bar{\mathrm{D}}_{i,j}}\right) \\ & + \frac{g\bar{\mathrm{D}}_{i,j}}{R\ \sin\theta}\frac{\Delta t}{\Delta\varphi}\left(h_{i+1,j}^n - h_{i,j}^n\right) \\ & - f\bar{N}_{i,j}^{n-\frac{1}{2}}\Delta t - \frac{gn^2}{\bar{D}_{i,j}^{7/3}}M_{i,j}^{n-\frac{1}{2}}\sqrt{M_{i,j}^{n-\frac{1}{2}2} + \bar{N}_{i,j}^{n-\frac{1}{2}2}}\Delta t \\ & + \frac{\bar{d}_{i,j}^2}{3R^2\sin^2\theta}\left(\frac{U^{n+\frac{1}{2}} - U^{n-\frac{1}{2}}}{\Delta\varphi^2} + \frac{\bar{V}^{n+\frac{1}{2}} - \bar{V}^{n-\frac{1}{2}}}{\Delta\theta\Delta\varphi}\right),\end{aligned} \tag{14}$$

where, again, because of the staggered grid system:

$$\bar{\mathrm{D}}_{i,j} = \frac{d_{i,j} + d_{i+1,j} + h_{i,j} + h_{i+1,j}}{2} \tag{15}$$

It should be noted that the 2nd and 3rd terms on the right-hand side of Eq. (14) were approximated with upwind finite differences.

Similarly, we considered the finite difference form for the dispersion term (the final term on the left-hand side) of Eq. (2):

$$\begin{aligned}&\frac{d^2}{3R}\frac{\partial}{\partial\theta}\left[\frac{1}{R\ \sin\theta}\left(\frac{\partial^2 M}{\partial\varphi\partial t} + \frac{\partial^2(N\ \sin\theta)}{\partial\theta\partial t}\right)\right] \\ &\quad = \frac{d^2}{3R^2}\frac{\partial}{\partial t}\left[\frac{\partial}{\partial\theta}\left(\frac{1}{\sin\theta}\frac{\partial M}{\partial\varphi}\right) + \frac{\partial}{\partial\theta}\left(\frac{1}{\sin\theta}\frac{\partial N\ \sin\theta}{\partial\theta}\right)\right]\end{aligned} \tag{16}$$

where:

$$\begin{aligned}\frac{\partial}{\partial\theta}\left(\frac{1}{\sin\theta}\frac{\partial M}{\partial\varphi}\right) &= \frac{\partial}{\partial\theta}\left(\frac{1}{\sin\theta}\frac{\bar{M}_{i+1,j} - \bar{M}_{i,j}}{\Delta\varphi}\right) \\ &= \frac{1}{\Delta\theta\Delta\varphi}\left(\frac{\bar{M}_{i+1,j} - \bar{M}_{i,j}}{\sin\theta} - \frac{\bar{M}_{i+1,j-1} - \bar{M}_{i,j-1}}{\sin(\theta-\Delta\theta)}\right),\end{aligned} \tag{17}$$

and because of the staggered grid system:

$$\bar{M}_{i,j} = \frac{M_{i,j} + M_{i,j+1} + M_{i-1,j} + M_{i-1,j+1}}{4}. \tag{18}$$

By further defining:

$$\bar{U} = \frac{\bar{M}_{i+1,j} - \bar{M}_{i,j}}{\sin\theta} - \frac{\bar{M}_{i+1,j-1} - \bar{M}_{i,j-1}}{\sin(\theta-\Delta\theta)}, \tag{19}$$

we can write:

$$\frac{\partial}{\partial t}\left[\frac{\partial}{\partial\theta}\left(\frac{1}{\sin\theta}\frac{\partial M}{\partial\varphi}\right)\right]=\frac{\partial}{\partial t}\left(\frac{\bar{U}}{\Delta\theta\Delta\varphi}\right)=\frac{\bar{U}^{n+\frac{1}{2}}-\bar{U}^{n-\frac{1}{2}}}{\Delta\theta\Delta\varphi\Delta t}. \tag{20}$$

The other term of Eq. (16) can be expressed as:

$$\begin{aligned}&\frac{\partial}{\partial\theta}\left(\frac{1}{\sin\theta}\frac{\partial N\ \sin\theta}{\partial\theta}\right)\\&=\frac{\partial}{\partial\theta}\left(\frac{1}{\sin\theta}\frac{N_{i,j+1/2}\sin(\theta+\Delta\ \theta/2)-N_{i,j-1/2}\sin(\theta-\Delta\ \theta/2)}{\Delta\theta}\right)\\&=\frac{1}{\Delta\theta}\frac{\partial}{\partial\theta}\left(\frac{N_{i,j+1/2}\sin(\theta+\Delta\ \theta/2)-N_{i,j-1/2}\sin(\theta-\Delta\ \theta/2)}{\sin\theta}\right)\\&=\frac{1}{\Delta\theta^2}\left(\frac{N_{i,j+1}\sin(\theta+\Delta\theta)-N_{i,j}\sin(\theta)}{\sin\left(\theta+\Delta\theta/2\right)}\right.\\&\quad\left.-\frac{N_{i,j}\sin(\theta)-N_{i,j-1}\sin(\theta-\Delta\theta)}{\sin\left(\theta-\Delta\theta/2\right)}\right).\end{aligned} \tag{21}$$

By defining:

$$\begin{aligned}V=&\frac{N_{i,j+1}\sin(\theta+\Delta\theta)-N_{i,j}\sin(\theta)}{\sin\left(\theta+\Delta\theta/2\right)}\\&-\frac{N_{i,j}\sin(\theta)-N_{i,j-1}\sin(\theta-\Delta\theta)}{\sin\left(\theta-\Delta\theta/2\right)},\end{aligned} \tag{22}$$

and we can write:

$$\frac{\partial}{\partial t}\left(\frac{\partial}{\partial\theta}\left(\frac{1}{\sin\theta}\frac{\partial N\ \sin\theta}{\partial\theta}\right)\right)=\frac{1}{\Delta\theta^2}\frac{\partial V}{\partial t}=\frac{V^{n+\frac{1}{2}}-V^{n-\frac{1}{2}}}{\Delta t\Delta\theta^2}. \tag{23}$$

By using Eqs. (20) and (23), the dispersion term of Eq. (2) can be expressed in finite-difference form as:

$$\begin{aligned}&\frac{d^2}{3R}\frac{\partial}{\partial\theta}\left[\frac{1}{R\ \sin\theta}\left(\frac{\partial^2 M}{\partial\varphi\partial t}+\frac{\partial^2(N\ \sin\theta)}{\partial\theta\partial t}\right)\right]\\&=\frac{\bar{d}_{i,j}^2}{3R}\left(\frac{\bar{U}^{n+\frac{1}{2}}-\bar{U}^{n-\frac{1}{2}}}{\Delta\theta\Delta\varphi\Delta t}+\frac{V^{n+\frac{1}{2}}-V^{n-\frac{1}{2}}}{\Delta t\Delta\theta^2}\right),\end{aligned} \tag{24}$$

where because of the staggered grid system:

$$\bar{d}_{i,j}=\frac{d_{i,j}+d_{i,j+1}}{2}. \tag{25}$$

Finally, Eq. (2) can be written in finite-difference form as:

$$\begin{aligned}N^{n+\frac{1}{2}}=&N^{n-\frac{1}{2}}-\frac{1}{R\ \sin\theta}\frac{\Delta t}{\Delta\varphi}\left(\frac{\bar{M}_{i,j+1}^{n-\frac{1}{2}}N_{i,j+1}^{n-\frac{1}{2}}}{\bar{\mathrm{D}}_{i,j+1}}-\frac{\bar{M}_{i,j}^{n-\frac{1}{2}}N_{i,j}^{n-\frac{1}{2}}}{\bar{\mathrm{D}}_{i,j}}\right)\\&+\frac{g\bar{\mathrm{D}}_{i,j}}{R}\frac{\Delta t}{\Delta\theta}\left(h_{i,j+1}^{n}-h_{i,j}^{n}\right)+f\bar{M}_{i,j}^{n-\frac{1}{2}}\Delta t\\&-\frac{gn^2}{\bar{D}_{i,j}^{7/3}}N_{i,j}^{n-\frac{1}{2}}\sqrt{\bar{M}_{i,j}^{n-\frac{1}{2}2}+N_{i,j}^{n-\frac{1}{2}2}}\Delta t\\&+\frac{\bar{d}_{i,j}^2}{3R^2}\left(\frac{\bar{U}^{n+\frac{1}{2}}-\bar{U}^{n-\frac{1}{2}}}{\Delta\theta\Delta\varphi}+\frac{V^{n+\frac{1}{2}}-V^{n-\frac{1}{2}}}{\Delta\theta^2}\right),\end{aligned} \tag{26}$$

where, because of the staggered grid system:

$$\bar{\mathrm{D}}_{i,j}=\frac{d_{i,j}+d_{i,j+1}+h_{i,j}+h_{i,j+1}}{2}. \tag{27}$$

It should also be noted that the 2nd and 3rd terms on the right-hand side of Eq. (26) are approximated with upwind finite differences.

Equation (3) can be written in the finite-difference form as:

$$\begin{aligned}h^{n+1}=&h^n-\frac{\Delta t}{R\ \sin\theta}\left[\left(\frac{\left(M_{i,j}^{n+\frac{1}{2}}-M_{i-1,j}^{n+\frac{1}{2}}\right)}{\Delta\varphi}\right.\right.\\&\left.\left.+\frac{\left(N_{i,j}^{n+\frac{1}{2}}\sin(\theta)-N_{i,j-1}^{n+\frac{1}{2}}\sin(\theta-\Delta\theta)\right)}{\Delta\theta}\right)\right].\end{aligned} \tag{28}$$

At time $t=n\Delta t$, we calculate $M^{n+1/2}$ and $N^{n+1/2}$ by substituting h^n, $M^{n-1/2}$, and $N^{n-1/2}$ into Eqs. (14) and (26). These equations are solved by use of an iterative method (Gauss–Seidel method) (Press *et al.* 1986). The calculated $M^{n+1/2}$ and $N^{n+1/2}$ are substituted into Eq. (28) to obtain h^{n+1}. Then h^{n+1}, $M^{n+1/2}$, and$N^{n+1/2}$ are used to solve Eqs. (14), (26), and (28) at the next time step.

References

Aida, I., *Reliability of a tsunami source model derived from fault parameters*, J. Phys. Earth, *26*, 57–73, 1978.

Ammon C.J., T. Lay, H. Kanamori, and M. Cleveland. 2011. *A rupture model of the 2011 off the Pacific coast of Tohoku Earthquake*, Earth Planets Space, *63*, 693–696, 2011.

Baba, T., N. Takahashi, Y. Kaneda, Y. Inazawa and M. Kikkojin, Tsunami inundation modeling of the 2011 Tohoku earthquake using three-dimensional building data for Sendai, Miyagi Prefecture, Japan, in V. S.-Fandiño *et al.* (ed.): Tsunami Events and

Lessons Learned, Advances in Natural and Technological Hazards Research, SPRINGER, *35*, 89–98, doi:10.1007/978-94-007-7269-4_3, 2014.

British Oceanographic Data Centre, GEBCO (General Bathymetric Chart of the Oceans). 2010. http://www.gebco.net/data_and_products/gridded_bathymetry_data, 2010.

Cerjan, C., D. Kosloff, R. Kosloff, and M. Reshef, *A nonreflecting boundary condition for discrete acoustic and elastic wave equations*, Geophysics, *50*, 705–708, doi:10.1190/1.1441945, 1985.

Fujitsu Corporation, press release, http://www.fujitsu.com/global/news/pr/archives/month/2011/20111102-02.html, 2012.

Goldstein, P., D. Dodge, M. Firpo, L. Minner, J. E. Tull, D. Harris, and W. C. Tapley, SAC—Seismic Analysis Code, http://www.iris.edu/manuals/sac/manual.html, 2007.

Goto, K., K. Fujima, D. Sugawara, S. Fujino, K. Imai, R. Tsudaka, T. Abe and T. Haraguchi, *Field measurements and numerical modeling for the run-up heights and inundation distances of the 2011 Tohoku-oki tsunami at Sendai Plain, Japan*, Earth Planets Space, *64*, 1247–1257, 2012.

Grilli, S.T., J.C. Harris, T.S.T. Bakhsh, T.L. Masterlark, C. Kyriakopoulos, J.T. Kirby and F. Shi, *Numerical simulation of the 2011 Tohoku tsunami based on a new transient FEM coseismic source: Comparison to far- and near-field observations*, Pure Appl. Geophys., *170*, 1333–1359, 2013.

Hayashi, Y., H. Tsushima, K. Hirata, K. Kimura, and K. Maeda, *Tsunami source area of the 2011 off the Pacific coast of Tohoku Earthquake determined from tsunami arrival times at offshore observation stations*, Earth Planets Space, *63*, 809–813, 2011.

Horillo, J., Kowalik, Z., Shigihara, Y., *Wave dispersion study in the Indian Ocean-tsunami of December 26, 2004*, Marine Geodesy, *29*, 149–166, 2006.

Imamura, F., S. Koshimura, T. Oie, Y. Mabchi, and Y. Murashima, Tsunami simulation for the 2011 off the Pacific coast of Tohoku Earthquake (Tohoku University model ver. 1.0), 12 pp., 2011.

Ito, T., K. Ozawa, T. Watanabe, and T. Sagiya. *Slip distribution of the 2011 off the Pacific coast of Tohoku Earthquake inferred from geodetic data*, Earth Planets Space, *63*, 627–630, 2011.

Iwase, H., Development of numerical model including dispersion effect from the tsunami source to the coastal area (in Japanese), PhD. thesis, 166p., 2005.

Jakeman, J.D., O.M., Nielsen, K., VanPutten, R., Mleczeko,, D. Burbidge, and N. Horspool, *Towards spatially distributed quantitative assessment of tsunami inundation models*, Ocean Dynamics, doi:10.1007/s10236-010-0312-4, 2010.

Japan Society of Civil Engineers, *Tsunami Assessment Method for Nuclear Power Plants in Japan*, JSCE, 321p., 2002.

Kido, Y., T. Fujiwara, T. Sataki, M. Kinoshita, S. Kodaira, M. Sano, Y. Ichiyama, Y. Hanafusa, S. Tsuboi. 2011. *Bathymetric feature around Japan Trench obtained by JAMSTEC multi narrow beam survey, MIS036-P58 (in Japanese)*, Japan Geoscience Union Meeting, 2011.

Kirby, J. T., F. Shi, B. Tehranirad, J. C. Harris, and S. T. Grilli, *Dispersive tsunami waves in the ocean: Model equations and sensitivity to dispersion and Coriolis effects*, Ocean Modelling, *62*, 39–55, 2013.

Løvholt, F., G. Kaiser, S. Glimsdal, L. Scheele, C. B. Harbitz, and G. Pedersen, *Modeling propagation and inundation of the 11 March 2011 Tohoku tsunami*, Nat. Hazards Earth Syst. Sci., *12*, 1017–1028, doi:10.5194/nhess-12-1017-2012, 2012.

Madsen, P.A., D.R. Fuhrman, and H.A. Schäffer, *On the solitary wave paradigm for tsunamis*, J. Geophys. Res., *113*, C12012, doi:10.1029/2008JC004932, 2008.

Maeda, T., T. Furumura, S. Sakai, and M. Shinohara, *Significant tsunami observed at ocean-bottom pressure gauges during the 2011 off the Pacific coast of Tohoku Earthquake*, Earth Planets Space, *63*, 803–808, 2011.

Matsuyama, M., M. Ikeno, T. Sakakiyama, and T. Takeda, *A study of tsunami wave fission in an undistorted experiment*, Pure Appl. Geophys., *164*, 617–631, doi:10.1007/s00024-006-0177-0, 2007.

Mori, N., *T. Takahashi and The 2011 Tohoku Earthquake Tsunami Joint Survey Group, Nationwide survey of the 2011 Tohoku earthquake tsunami*, Coastal Engineering Journal, *54*, 1–27, 2012.

Murashima, Y., S. Koshimura, H. Oka, Y. Murata, K. Fujima, H. Sugino, Y. Iwabuchi, *Numerical simulation of soliton fission in 2011 Tohoku tsunami using nonlinear dispersive wave model, (in Japanese with English abstract)*, J. Japan Society of Civil Engineers (B2), *68*, I_206–I_212, 2012.

Murashima, Y., S. Koshimura, H. Oka, Y. Murata, and F. Imamura, *Development of the practical river run-up model of tsunami based on non-linear dispersive wave theory (in Japanese)*, J. Japan Society of Civil Engineers (B2), *66*, 201–205, 2010.

Nishimura, T., H. Munekane, and H. Yarai, *The 2011 off the Pacific coast of Tohoku Earthquake and its aftershocks observed by GEONET*, Earth Planets Space, *63*, 631–636, 2011.

Peregrine, H., *Equations for water waves and the approximations behind them*, edited by R. E. Meyer, pp. 95–121, Waves on Beaches and Resulting Sediment Transport, Academic Press, New York, 1972.

Press, W. H., B. P. Flannery, S. A. Teukolsky, and W. T. Vetterling, *Numerical Recipes*, Cambridge Univ. Press, Cambridge, 1986.

Roeber, V., Cheung, K. F., and Kobayashi, M. H., *Shock-capturing Boussinesq-type model for nearshore wave processes*, Coastal Engineering, *57*, 407–423, 2010.

Saito T., K. Satake, and T. Furumura, *Tsunami waveform inversion including dispersive waves: the 2004 earthquake off Kii Peninsula, Japan*, J. Geophys. Res., *115*, B06303, doi:10.1029/2009JB006884, 2010.

Saito, T., Y. Ito, D. Inazu, and R. Hino, *Tsunami source of the 2011 Tohoku-Oki earthquake, Japan: Inversion analysis based on dispersive tsunami simulations*, Geophys. Res. Lett., *38*, L00G19, doi:10.1029/2011GL049089, 2011.

Shao, G, X. Li, C. Ji, and T. Maeda, *Focal mechanism and slip history of 2011 Mw 9.1 off the Pacific coast of Tohoku earthquake, constrained with teleseismic body and surface waves*, Earth Planets Space, *63*, 559–564, 2011.

Satake, K. Tsunamis, in International Handbook of Earthquake and Engineering Seismology, (eds. Lee,W.H.K., Kanamori, H., Jennings, P.C., and Kisslinger, C.), Academic Press, *81A*, 437–451, 2002.

Satake, K., Y. Fujii, T. Harada, and Y. Namegaya, *Time and space distribution of coseismic slip of the 2011 Tohoku earthquake as inferred from tsunami waveform Data*, Bull. Seismol. Soc. Am., *103*, 1473–1492, doi:10.1785/0120120122, 2013.

Shigihara, Y., and Fujima K., *Wave dispersion effect in the Indian ocean tsunami*, J. Disaster Research, *1*, 142–147, 2006.

Shuto, N., *The Nihonkai-Chubu earthquake tsunami on the north Akita coast (in Japanese)*, Costal Engin. Japan JSCE 28, Tokyo, Japan, 255–264, 1985.

Sitanggang K. I. and Lynett, P., *Parallel computation of a highly nonlinear Boussinesq equation model through domain decomposition*, Int. J. Numer. Fluids, *49*, 57–74, 2005.

Son, S., Lynett, P., Kim, D.-H., *Nested and multi-physics modeling of tsunami evolution from generation to inundation*, Ocean Modell. *38*, 96–113, doi:10.1016/j.ocemod.2011.02.007, 2011.

Suito, H., T. Nishimura, M. Tobita, T. Imakiire, and S. Ozawa, *Interplate fault slip along the Japan Trench before the occurrence of the 2011 off the Pacific coast of Tohoku Earthquake as inferred from GPS data*, Earth Planets Space, *63*, 615–619, 2011.

Takagawa, T., and T. Tomita, *Tsunami source inversion with time evolution and real-time estimation of permanent deformation at observation points*, J. Japan Society of Civil Engineers (B2), *68*, I_311–I_315, 2012.

Tsushima, H., R. Hino, Y. Tanioka, F. Imamura, H. Fujimoto, *Tsunami waveform inversion incorporating permanent seafloor deformation and its application to tsunami forecasting*, J. Geophys. Res., *117*, B03311, doi:10.1029/2011JB008877, 2012.

Wessel, P., Smith, W.H.F., *New, improved version of generic mapping tools released*, EOS Trans., AGU79, 579, 1998.

Yagi, Y. and Y. Fukahata, *Rupture process of the 2011 Tohoku-oki earthquake and absolute elastic strain release*, Geophys. Res. Lett., *38*, L19307, doi:10.1029/011GL048701, 2011.

Zhou, H., C. W. Moore, Y. Wei, and V. V. Titov, *A nested-grid Boussinesq-type approach to modeling dispersive propagation and runup of landslide-generated tsunamis*, Nat. Hazards Earth Syst. Sci., *11*, 2677–2697, doi:10.5194/nhess-11-2677-2011, 2011.

(Received February 19, 2014, revised February 3, 2015, accepted February 4, 2015, Published online February 21, 2015)